A Study of the Relationship Between the Dynamic Factors and the Dynamic Transmission Error of Spur Gear Pairs

V. K. Tamminana

A. Kahraman[1]
e-mail: kahraman.1@osu.edu

Department of Mechanical Engineering,
The Ohio State University,
206 W. 18th Avenue,
Columbus, OH 43210

S. Vijayakar
Advanced Numerical Solutions,
3956 Brown Park Drive, Suite B,
Hilliard, OH 43026

In this study, two different dynamic models, a finite-element-based deformable-body model and a simplified discrete model, are developed to predict dynamic behavior of spur gear pairs. Dynamic transmission error (DTE) and dynamic factors (DF) defined based on the gear mesh loads, tooth loads and bending stresses are computed for a number of unmodified and modified spur gears within a wide range of rotational speed for different involute contact ratios and torque values. Although similar models were proposed in the past, they were neither fully validated nor equipped to predict both DTE and different forms of DF. Accordingly, this study focuses on (i) validation of both models through an extensive set of experimental data obtained from a set of tests using spur gear having unmodified and modified tooth profiles, and (ii) establishment of a direct link between DTE and different forms of DF, especially the ones based on tooth forces and the root stresses. The predicted DF and DTE values are related to each other through simplified formulas. Impact of nonlinear behavior, such as tooth separations and jump discontinuities on DF, is also quantified. [DOI: 10.1115/1.2359470]

1 Introduction

Dynamic behavior of gear systems is important for two main reasons. One reason is the durability of the gear pair. Forces acting at the gear meshes and bearings under dynamic conditions might be many times larger than corresponding quasi-static forces. As a result of this, stresses, and hence, bending and contact fatigue lives of a gear set are influenced by its vibratory behavior. Gear design standards incorporate a dynamic rating factor [1] in an attempt to account for such dynamic effects. The second reason that makes the dynamic behavior relevant is the noise generated by the gear set. Time-varying dynamic gear mesh and bearing forces are transmitted to surrounding structures through the housing and the mounts to cause gear whine noise. Therefore, large vibration amplitudes typically result in higher noise levels as well.

Most of the theoretical and experimental studies to date were performed with only one of the reasons (noise or durability) in mind. Starting with the dynamic models, a large number of them have been developed over the years as reviewed by Ozguven and Houser [2], Blankenship and Singh [3], and Wang et al. [4]. A great majority of these studies uses discrete models to predict the parameters that might be useful in quantifying how noisy the gear set would be. A few examples from a large number of studies of this type are referenced here to represent this approach [5–13]. A discrete gear mesh interface model consists of a mesh stiffness element (mostly a periodically time-varying one to represent the fluctuation of the number of tooth pairs in contact as gears rotate) and a viscous damper that are both applied along the line of action of the spur gear pair. A clearance-type constraint to represent backlash-induced tooth separations and an external displacement excitation to represent gear profile errors and intentional tooth modifications were included in some of these models. Both mesh stiffness function and displacement excitation would be determined by using a static-elastic gear analysis model. One commonly used form output from these models was the dynamic transmission error (DTE) that is defined as

$$\mathrm{DTE} = r_1\theta_1(t) + r_2\theta_2(t) \tag{1}$$

which represents the motion transfer error along the line of action of gears where r_1 and r_2 are the base radii of gears 1 and 2, and $\theta_1(t)$ and $\theta_2(t)$ are the alternating components of angular displacements that are measured from the nominal positions of gears at a given rotational speed. This is the dynamic equivalent of the better known static transmission error (STE). A number of major experimental studies on spur gear dynamics, including Munro [14], Umezawa et al. [15], and Blankenship and Kahraman [16–20] used DTE as the metric to quantify the dynamic behavior. These experimental studies demonstrated clearly that mesh stiffness fluctuations and gear backlash must be included in an analysis of a spur gear pair as it acts as a parametrically excited nonlinear system in dynamic terms. These experimental studies guided many modeling efforts and were used extensively for modal validation efforts [6–8,16,17].

Several other investigations predicted dynamic forces acting at the gear mesh to quantify the dynamic behavior [21–27]. Since the gear mesh damping force is very small compared to the gear mesh spring force, the dynamic gear mesh force (DMF) can be approximated as the product of the gear mesh stiffness and DTE. Dynamic factor was defined in these studies as $\mathrm{DF} = (\mathrm{DMF})_{\max}/\mathrm{SMF}$, where $(\mathrm{DMF})_{\max}$ is the maximum value of the dynamic mesh force and SMF is the static mesh force transmitted by the gear pair. The main shortcoming of these models is that they were capable of predicting only DF based on the gear mesh forces as defined earlier, whereas the durability of the system would require prediction of the state of gear stresses under dynamic conditions. An accurate prediction of dynamic stresses requires the dynamic model that includes flexible teeth, gear blanks, and contacts, all of which are possible via a deformable body model. There are recent deformable-body spur gear dynamics models (e.g., [28]), which were shown to compare well with DTE measurements of some of the studies cited earlier [16–20]. How-

[1]Corresponding author.

Contributed by the Power Transmission and Gearing Committee of ASME for publication in the JOURNAL OF MECHANICAL DESIGN. Manuscript received June 10, 2005; final manuscript received February 12, 2006. Review conducted by Teik C. Lim. Paper presented at the ASME 2005 Design Engineering Technical Conferences and Computers and Information in Engineering Conference (DETC2005), September 24–28, 2005, Long Beach, California, USA.

ever, these deformable-body models did not focus on DF or gear stresses as a part of the dynamic behavior. Similarly, experimental studies that focused on the measurement of the dynamic bending gear stresses [29] are yet to be related to any dynamic model.

This study attempts to bridge this apparent gap between gear durability concerns and gear dynamics models. Specific objectives are

1. to develop and validate dynamic models to predict DTE and all forms of DF, simultaneously,
2. to investigate the relationships between DTE and different forms of DF, and
3. to quantify the influence of tooth separations on DF values.

For this purpose, two different dynamic models, a deformable-body model and a discrete model, will be developed. The deformable-body model will have the capacity of predicting both DTE and DF based on mesh and tooth forces as well as dynamic gear tooth bending stresses. The discrete model will rely on the deformable-body model for computation of gear mesh parameters under quasi-static conditions and will predict both DTE and DF based on mesh and tooth forces. A set of spur gear experiments will be employed to validate both models by comparing predicted and measured DTE values. The validation matrix will include several gear sets having different involute contact ratios and tooth-profile modifications operating within a wide range of rotational speed at different applied loads. The validated models will then be used for two specific purposes. First, DTE values will be related to DF values based on (i) gear mesh forces, (ii) tooth forces, and (iii) bending stresses. Simplified relationships between DTE and different forms of DF will be proposed, with the intent that extensive experimental and theoretical DTE database available in the literature can be related to the durability of the gear sets. Second, the impact of tooth separations and jump discontinuities due to backlash on gear stresses will be quantified. Such effects were studied in the past using DTE solely for noise purposes, and their impact on gear durability is yet to be understood.

2 Dynamic Models

2.1 Deformable-Body Model. The width of the contact zone in typical gear applications is two orders of magnitude smaller than the dimensions of the gear teeth themselves, requiring a very fine mesh inside the contact zone. The location of the contact zone changes as the gears enter and exit the mesh. When conventional finite element (FE) methods are used, besides having an extremely refined mesh, re-meshing is necessary for every contact position.

A gear contact analysis model [30], which is the same model used in Ref. [28], will be used here to perform a deformable-body dynamic analysis of a spur gear pair. The model divides the gear into a near-field region near the contact and a far-field region away from the contact. The FE method is used to compute relative deformations and stresses for points in the far-field, and a semi-analytical deformation model based on the Bousinesq and Cerruti solutions is used in the near field within the contact zones [31]. This approach does not require a highly refined mesh at the contacting tooth surfaces, reducing the computational effort compared to conventional FE models, which require a refined mesh at gear tooth region, limiting the model to static analysis only. Therefore, the model used here allows a more refined and comprehensive study of spur gear dynamics than the conventional FE models. The tooth surfaces are modeled by a large number of nodes representing the involute shape and surface modifications. The model illustrated in Fig. 1 makes it unnecessary to locally refine the FE mesh near the contact, and remesh the finite elements for each contact position.

A reference frame is attached to the pinion and gear, and the finite element computations are done for each of them separately. The mesh stiffness and mesh contact forces, comprising the dynamic excitation for the system, are evaluated internally at each time step [31]. Contact conditions are handled as linear inequality constraints whose solution is obtained by a revised SIMPLEX solver.

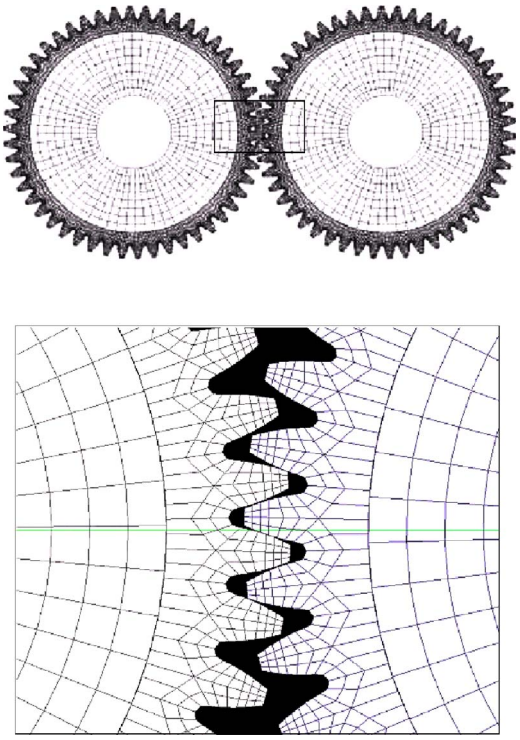

Fig. 1 Deformable-body dynamic model of an example spur gear pair

Contact analysis determines the contact conditions between the pinion and gear at each time step. In the absence of rigid-body motion, the FE displacement vector $\mathbf{x}_{fi}$ for gear i satisfies the linear system of differential equations [28]

$$\mathbf{M}_{ffi}\ddot{\mathbf{x}}_{fi} + \mathbf{C}_{ffi}\dot{\mathbf{x}}_{fi} + \mathbf{K}_{ffi}\mathbf{x}_{fi} = \mathbf{f}_{fi} \tag{2}$$

where $\mathbf{f}_{fi}$ is the vector of external loads. Rayleigh's damping model is used here in the form $\mathbf{C}_{ffi} = \mu\mathbf{M}_{ffi} + \eta\mathbf{K}_{ffi}$, where μ and η are constant coefficients. If rigid-body motion is considered, and if we represent the rigid-body degrees of freedom by $\mathbf{x}_{ir}$, we replace Eq. (2) by

$$\begin{bmatrix} \mathbf{M}_{ffi} & \mathbf{M}_{fri} \\ \mathbf{M}_{rfi} & \mathbf{M}_{rri} \end{bmatrix} \begin{Bmatrix} \ddot{\mathbf{x}}_{fi} \\ \ddot{\mathbf{x}}_{ri} \end{Bmatrix} + \begin{bmatrix} \mathbf{C}_{ffi} & \mathbf{C}_{fri} \\ \mathbf{C}_{rfi} & \mathbf{C}_{rri} \end{bmatrix} \begin{Bmatrix} \dot{\mathbf{x}}_{fi} \\ \dot{\mathbf{x}}_{ri} \end{Bmatrix} + \begin{bmatrix} \mathbf{K}_{ffi} & \mathbf{K}_{fri} \\ \mathbf{K}_{rfi} & \mathbf{K}_{rri} \end{bmatrix} \begin{Bmatrix} \mathbf{x}_{fi} \\ \mathbf{x}_{ri} \end{Bmatrix} = \begin{Bmatrix} \mathbf{f}_{fi} \\ \mathbf{f}_{ri} \end{Bmatrix} \tag{3}$$

The equations for the pinion ($i=1$) and the gear ($i=2$) are assembled into the matrix equation of motion for the system:

$$\mathbf{M}\ddot{\mathbf{x}} + \mathbf{C}\dot{\mathbf{x}} + \mathbf{K}\mathbf{x} = \mathbf{F} \tag{4}$$

The deformable body model employs a time-discretization scheme based on Newmark method [30], as used successfully in previous studies [28,32].

2.2 Discrete Parameter Model. The proposed discrete model is based on an existing gear dynamics model developed by one of these authors [16]. This nonlinear, time-varying model is shown in Fig. 2. It consist of two rigid wheels of polar mass moments of inertia of I_1 and I_2, and base radii of r_1 and r_2. The gear mesh interface is represented by a periodically time-varying mesh stiffness function $k(t)$ and a viscous damper c. Here $k(t)$ takes into account the parametric excitation due to the mesh stiffness varia-

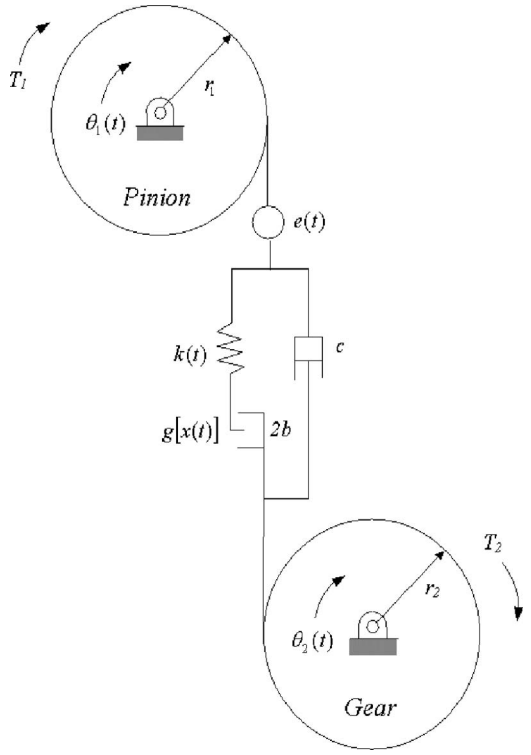

Fig. 2 Discrete dynamic model a spur gear pair

tion caused by the fluctuation of number of tooth pairs in contact. A clearance-type nonlinear restoring function g is included to represent the gear backlash of magnitude $2b$. An external displacement excitation $e(t)$ is also applied at the gear mesh interface to represent manufacturing errors and intentional modifications of the tooth profile. Friction forces at the gear tooth contact are neglected, and the shafts and bearings supporting the gears are assumed to be rigid. In Fig. 2, the alternating rotational displacements $\theta_1(t)$ and $\theta_2(t)$ are defined positive in clockwise direction. With these assumptions, the equation of motion represented by the single-degree-of-freedom dynamic model shown in Fig. 2 is given for a coordinate $x(t)=r_1\theta_1(t)+r_2\theta_2(t)-e(t)$ as

$$m_e\ddot{x}+c\dot{x}+k(t)g[x(t)]=F-m_e\ddot{e}(t) \tag{5a}$$

$$g[x(t)]=\begin{cases}x(t)-b, & x(t)>b\\ 0, & |x(t)|\leq b\\ x(t)+b, & x(t)<-b\end{cases} \tag{5b}$$

$$F=m_e\left(\frac{T_1r_1}{I_1}+\frac{T_2r_2}{I_2}\right) \tag{5c}$$

$$m_e=\frac{I_1I_2}{I_1r_2^2+I_2r_1^2} \tag{5d}$$

where an overdot denotes differentiation with respect to time t, and T_1 and T_2 are constant torque values applied to the pinion and gear, respectively. Torque fluctuations are not considered in this model as the experimental setup described later is suitably designed to maintain a constant torque value. In Eq. (5), $x(t)$ represents the difference between DTE defined in Eq. (1) and the unloaded STE.

The governing equation (5) can be nondimensionalized by defining a characteristic frequency $\omega_n=\sqrt{k_m/m_e}$ and a characteristic displacement b (half backlash). Here, ω_n is the undamped natural frequency of the corresponding linear time-variant system where

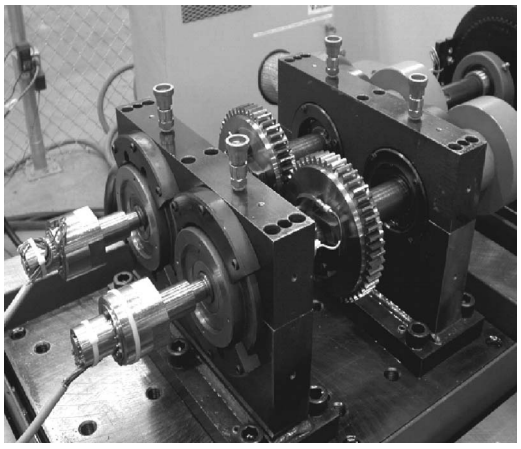

Fig. 3 Gear dynamics test machine

k_m is the mesh stiffness, i.e., $k(t)=k_m+k_a(t)$. Defining a dimensionless time $\tau=\omega_n t$, a viscous damping ratio $\zeta=c/(2\sqrt{m_ek_m})$ and dimensionless displacements $\bar{x}(\tau)=x(\tau)/b$ and $\bar{e}(\tau)=e(\tau)/b$, one obtains

$$\bar{x}''+2\zeta\bar{x}'+[1+\bar{k}_a(\tau)]g[\bar{x}(\tau)]=f-\bar{e}''(\tau) \tag{6a}$$

$$g[\bar{x}(\tau)]=\begin{cases}\bar{x}(\tau)-1, & \bar{x}(\tau)<1\\ 0, & |\bar{x}(\tau)|\leq 1\\ \bar{x}(\tau)+1, & \bar{x}(\tau)>-1\end{cases} \tag{6b}$$

where $f=F/(k_mb)$, $\bar{k}_a(\tau)=k_a(\tau)/k_m$, and $(\,)'$ denotes differentiation with respect to τ.

One of the main disadvantages of this model is its dependence on the deformable-body model to determine the gear mesh parameters $k(t)$ and $e(t)$. The involute profile modifications are represented in this model by $e(t)$ that corresponds to unloaded STE. Hence, a static analysis is performed on the deformable-body model developed for the same gear pair, described in detail in Sec. 2.1, under unloaded conditions for several discrete positions over a period of one mesh cycle to determine $e(t)$. Similarly, the mesh stiffness function $k(t)$ is obtained from the same static analysis of the deformable-body model, now under operating load conditions. As the gears rotate, the number of teeth in contact changes resulting in time-varying mesh stiffness. This analysis is repeated at the same discrete rotational positions over a mesh cycle to obtain the loaded static transmission error (LSTE). This is used to estimate the mesh stiffness at each discrete position i as

$$k_i=\frac{T_1}{r_1}\left[\frac{1}{(\mathrm{LSTE}-e)_i}\right] \tag{7}$$

Both $e(t)$ and $k(t)$ are represented in Fourier series form in the model. The nonlinear differential equation of motion (6) is solved numerically by using a fourth-order, variable-step Runge-Kutta (Dormand-Prince pair) numerical integration routine available in MATLAB.

It should be pointed out that this discrete model employs a number of simplifying assumptions, rigid gear blank assumption perhaps being the most critical one. Therefore, this model should be expected to be reasonably accurate only for the applications where the gear rims are quite rigid. In cases when this is not true, a deformable-body model should be considered as the only accurate model to predict gear dynamic behavior.

3 Validation of Dynamic Models

3.1 Experimental Study. A power-circulation-type test machine shown in Fig. 3 is employed for the experimental study. The

Fig. 4 The test gear pairs used in this study: (*a*) δ=0, ICR =1.8; (*b*) δ=10 μm, α=20.9 deg, ICR=1.8; and (*c*) δ=0, ICR =1.4

same test machine was used previously to study nonlinear behavior of spur gear pairs including jump discontinuities, parametric resonances, and chaotic motions [16–18]. Experimental investigations on the influence of certain design parameters, such as tooth profile modifications [19] and contact ratio [20], on the dynamic behavior of spur gear pair were also performed using the same machine. A detailed description of the test machine can be found in [16]. It is of primary interest here to note that the test gear set shown to the left in Fig. 3 are well isolated from the reaction gear box through massive flywheels, elastomer couplings, and flexible shafts, such that influence of the reaction gear pair on the dynamic behavior of the test gear system is negligible. A constant torque is applied to the closed loop thorough a split coupling. Each test gear is assembled on its shaft precisely to avoid any mounting error. A pair of precision spherical roller bearings supports the bearings that are housed in the bearing caps. The bearing caps and the bearings pedestals are such that there are no shaft misalignments. In addition, the bearing pedestals and the bedplate of the test machine are rigid.

A rotational speed range of 500–4000 rpm (415–3330 Hz of mesh frequency) is considered for each test. The accelerometer-based DTE measurement system consists of four diametrically opposed linear accelerometers on each test gear shaft that are mounted near the gear blanks tangentially at a certain radius such that $\ddot{\theta}_1$ and $\ddot{\theta}_2$ can be measured with any gravitational effects cancelled out. These signals are combined using analog circuitry to obtain $d^2(\mathrm{DTE})/dt^2 = r_1\ddot{\theta}_1 + r_2\ddot{\theta}_2$, which is integrated twice to obtain DTE. Details of this method and the signal processing can be found in [16].

Different sets of spur test gear pairs are considered in the experimental study representing different modification parameters and involute contact ratios (ICR). Experimental test matrix covered an ICR range between 1.0 and 2.0 as well as different magnitudes of linear profile tip relief (δ=0,4, and 10 μm) and different roll angles where the tip relief starts (α=20.9 deg representing the pitch point, α=22.2 deg near the highest point of single tooth contact, α=23.6 deg and α=24.8 deg). Because of space limitations, this paper will use data from a small subset of this experimental study formed by the three gear pairs shown in Fig. 4. Table 1 lists the common gear design parameters of the test gears. Each gear pairs are formed by identical gears (unity ratio) and operated at a 150 mm center distance.

Each gear set was tested at several torque levels up to 350 N-m; however, only the results for 170 Nm and 340 Nm are included in this paper. The rotational speed was varied between 500 rpm and 4000 rpm with an increment of nearly 50 rpm and

Table 1 Common design parameters of the spur gear pairs used for the model validation

Number of teeth	50
Module, mm	3.0
Pressure angle, deg	20.0
Pitch diameter, mm	150.0
Base diameter, mm	140.954
Outside diameter, mm	variable
Normal circular tooth thickness, mm	4.64
Helix angle, deg	0
Tooth profile modifications	variable

root-mean-square (rms) value of the measured DTE at each speed increment was recorded under steady state conditions. In order to capture jump-up- and jump-down-type nonlinear phenomena, tests were repeated for both speed-up and speed-down conditions.

3.2 Comparison of Measured and Predicted DTE Values. Dynamic analyses are performed using both models for different sets of gear pairs described in Sec. 3.1. The models are validated by comparing the predicted DTE values to the measured ones. The deformable-body model for one of the example gear pairs is shown in Fig. 1. Lumped inertias were added to the gear inertias to account for the difference in the width between gear teeth and the blank. The Rayleigh damping coefficients were chosen as μ =479 and $\eta = 1.4(10)^{-7}$ [28] so that the damping ratio is ~1% as determined by the experiments.

In order to capture jump-up- and jump-down-type nonlinear phenomena as in experiments, simulations were also repeated for both speed-up and speed-down conditions within a range of 500–4000 rpm (gear mesh frequency 415–3330 Hz) with a increment between 50 rpm and 150 rpm. In order to reach steady-state motions, each deformable-body analysis was performed in four different stages. First, the system was ramped up (or down) to the desired speed in a relatively smaller number of very coarse time steps (25 mesh cycles with 8 time steps per mesh cycle). A second stage of simulation was performed at this constant speed to surpass the transients using a coarse time step (30–50 mesh cycles with ~20 time steps per mesh cycle), followed by a more refined third stage (25 mesh cycles with 50 points per mesh cycle) to reach steady-state motions. The final stage of simulation used a very small time step (4 mesh cycles with 128 points per mesh cycle) to capture all dynamic motions to the desired resolution. This final section of data was used to extract steady-state response. Here, the main reason for performing the last two stages separately was that stress calculations increase the computational time by more than a factor of two. Hence, by enabling stress calculations only in the final stage of analysis, significant amount of computational effort was saved without compromising the required resolution of response. As in the case of an actual speed sweep, the last simulation point of the steady-state motion from the previous speed increment was considered as the initial condition for the ramp-up (ramp-down) followed by a refined steady-state simulation.

For the discrete model simulation, gear inertias are calculated using the disk approximation as 0.0073 kg-m^2 and gear mesh parameters are obtained from the quasi-static analysis of deformable-body model. Speed changes were introduced in sudden step increments. However, since the simulation is extremely fast compared to that of the deformable-body model, a much smaller speed increment was used and the simulation at each speed increment was carried out with a refined time step (~125 mesh cycles with 128 points per mesh cycle).

In the deformable-body model, time histories of DTE were calculated from the angular displacements of the pinion and gear using Eq. (1). Time histories of the dynamic mesh force (DMF) were obtained by adding all the individual dynamic tooth forces (DTF). Fast Fourier transform (FFT) of the each time history is used to compute the root-mean-square (rms) values of DTE and

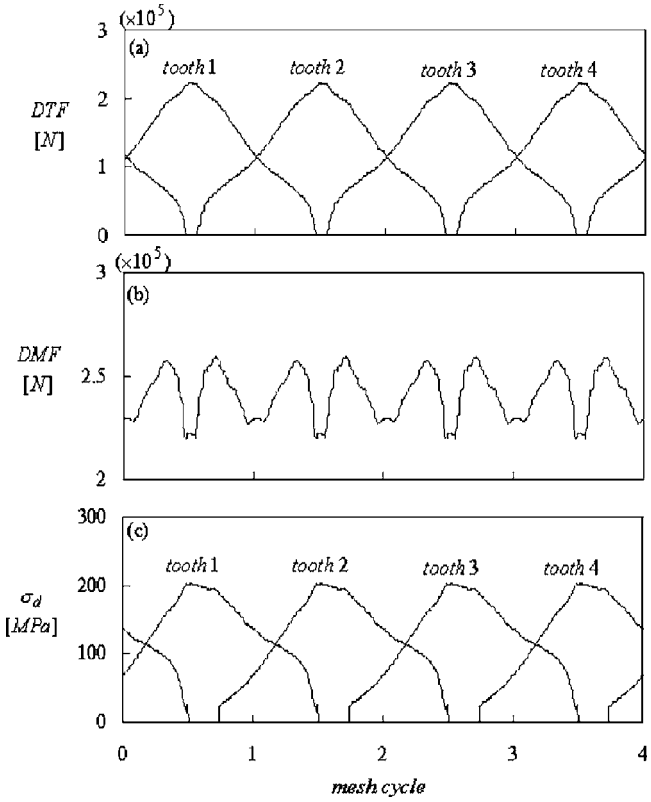

Fig. 5 Time histories of (*a*) dynamic tooth force, (*b*) dynamic mesh force, and (*c*) dynamic max principal stress at 2 kHz for a modified gear pair with δ=10 μm, α=20.9 deg, and ICR=1.8 at 340 Nm using deformable body model

DMF. Maximum principal stresses, $\sigma_{\max}$, were computed at several predetermined root locations ranging from the root center to the start of active profile. Figure 5 illustrates time histories of DTF, DMF, and maximum principal stress at 2 kHz for a modified gear pair with δ=10 μm and α=20.9 deg, computed by using the deformable-body model.

In the case of the discrete model, DMF at a given time τ is defined as

$$\mathrm{DMF}(\tau) = k_m b\{2\zeta\bar{x}' + [1 + \bar{k}_a(\tau)]g[\bar{x}(\tau)]\} \tag{8}$$

Here, it may be noted that the magnitude of the damping force term is very small compared to the mesh stiffness force term and, hence, may be neglected in the calculation of the total gear mesh force. Individual dynamic tooth forces (DTF) were calculated using an approximate formula given by

$$\mathrm{DTF}(\tau) = \left[\frac{\mathrm{STF}(\tau)}{\mathrm{SMF}}\right]\mathrm{DMF}(\tau) \tag{9}$$

The static tooth force STF(τ) is obtained from the deformable-body model for one complete mesh cycle under quasi-static conditions.

Data from three gear sets shown in Fig. 4 are presented here for validation of the models. In Fig. 6 for the first gear pair having no profile modification (δ=0) and ICR=1.8 at 340 Nm, the rms values of the measured DTE are compared to predictions of both models within the entire mesh frequency range of interest. It is observed in Fig. 6 that the predictions of the deformable-body model match measured data very well in terms of both overall amplitudes and the shape of the forced response. The measured primary resonance near 3100 Hz as well as the first two superharmonic resonances near 1550 Hz and 1000 Hz are predicted accurately by the deformable-body model. The amplitudes of the DTE

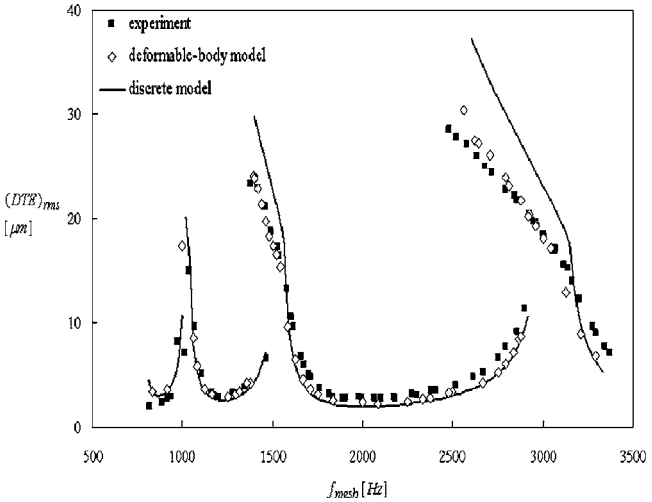

Fig. 6 Comparison of measured and predicted rms values of DTE for an unmodified gear pair with δ=0 and ICR=1.8 at 340 Nm

are also predicted accurately in both resonance and off-resonance regions. In addition, the measured nonlinear behavior characterized by a frequency range of double stable motions (a lower-branch no-contact-loss motion and an upper-branch tooth-separation motion) bounded by jump-up and jump-down discontinuities also match well with the experimental data. The same conclusions can also be reached for the discrete model with one exception that the DTE predictions of this model along the upper-branch tooth-separation motions are somewhat larger than the experimental data as well as the deformable-body model predictions. This might be because the model shown in Fig. 2 is a very simple one with many secondary effects neglected, including gear blank deflections.

Figures 7 and 8 present the same type comparison for the other two gear pairs at 340 Nm and 170 Nm, respectively. In Fig. 7 for an ICR=1.8 gear pair with a linear tip relief of δ=10 μm starting at the pitch line (α=20.9 deg roll angle), the nonlinear behavior is significantly less and the forced response is nearly linear. This is attributed to the fact that the applied load of 340 Nm corresponds to the "design load" for the profile modifications made on the gear pair [19]. Because of this, the discrete model compares to experi-

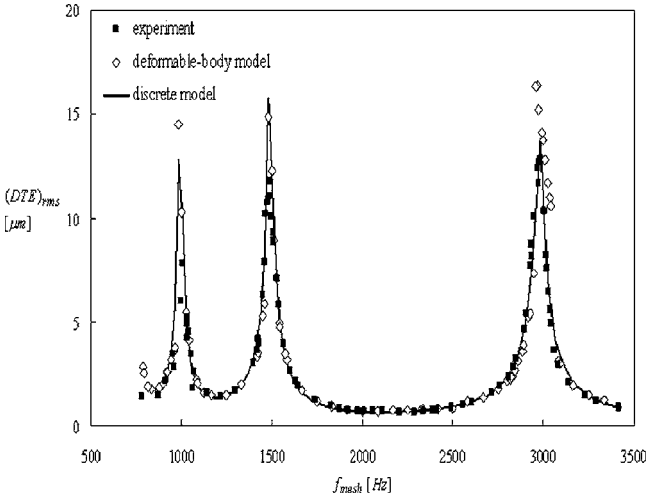

Fig. 7 Comparison of measured and predicted rms values of DTE for a modified gear pair with δ=10 μm, α=20.9 deg, and ICR=1.8 at 340 Nm

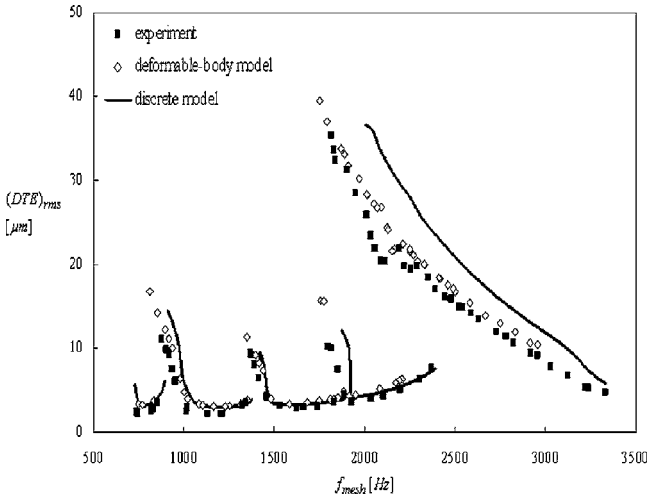

Fig. 8 Comparison of measured and predicted rms values of DTE for an unmodified gear pair with δ=0 and ICR=1.4 at 170 Nm

ments as good as the deformable-body model. Meanwhile, the nonlinear jump discontinuities due to tooth separations are again evident in Fig. 8 for the third gear pair having no profile modifications (δ=0) but a different involute contact ratio, ICR=1.4 at 170 Nm. Similar to Fig. 6, both models compare well to the measured data, whereas the discrete model predicts larger upper-branch motions with separations. In addition to the good agreement in terms of the rms values of DTE, the harmonic components of predicted DTE also compare well to the experiment. Figure 9 illustrates this for the gear pair used in Fig. 7 at three different gear mesh frequencies of 1.5, 2.1, and 2.9 kHz.

Comparisons to experimental data from gear pairs having parameters different from those shown in Fig. 4 were also made in this study with the same level of agreement. For instance, gear pairs having other ICR values and different modification amplitudes (say, δ=4 μm) were tested and simulated at torque levels other than the ones considered here to demonstrate that both models are indeed capable of predicting the dynamic response of a gear pair accurately. These additional comparisons can be found in [33].

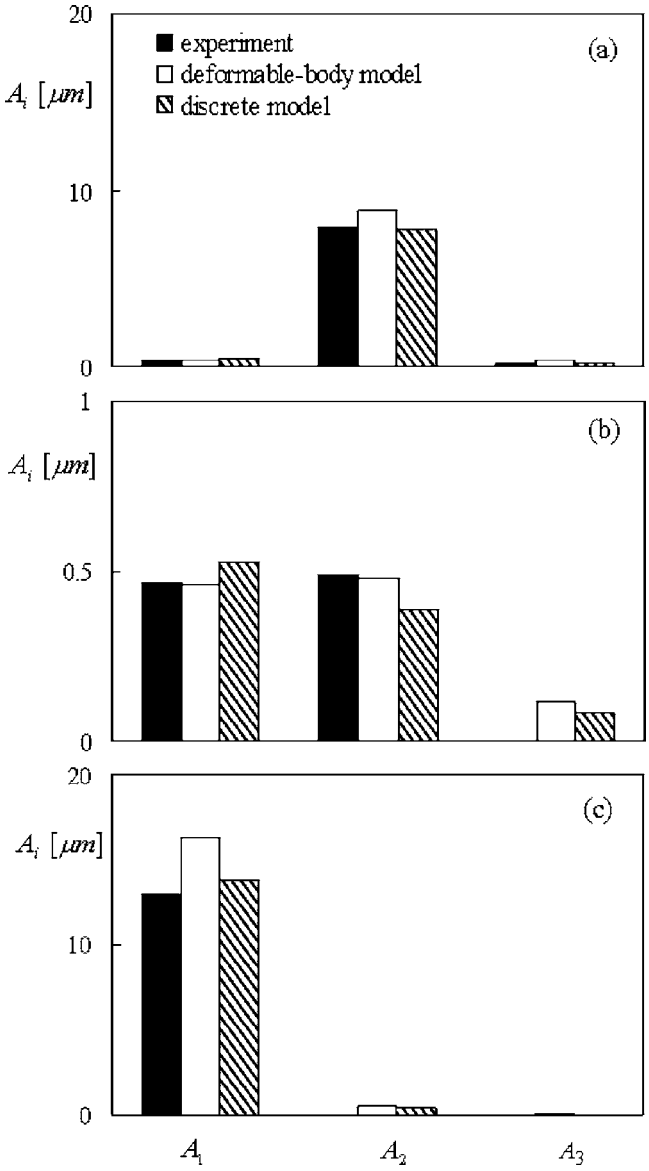

Fig. 9 Comparison of the harmonic amplitudes of measured and predicted DTE for δ=10 μm, α=20.9 deg, and ICR=1.8 at 340 Nm: (*a*) 1500 Hz, (*b*) 2100 Hz, and (*c*) 2900 Hz

4 Comparison of DTE and Different Forms of DF

Next, the validated dynamic models introduced earlier will be used to investigate the relationship between the DTE, a commonly measured and predicted noise metric, and different forms of dynamic factors that have been used in design to account for the increase in forces and bending stresses due to dynamic effects. Before this can be done, different versions of DF will be defined here based on the total gear mesh force, individual tooth forces, and the principal bending stresses. The dynamic mesh force factor $(DF)_{mf}$ will be defined as the ratio of the maximum value of the dynamic mesh force in one complete mesh cycle of the steady-state response to the static mesh force

$$(DF)_{mf} = \frac{(DMF)_{max}}{SMF} \tag{10a}$$

where SMF=$T_1/r_1=T_2/r_2$=const. Similarly, the dynamic tooth force factor $(DF)_{tf}$ is the ratio of the maximum value of the dynamic tooth force in one complete mesh cycle of the steady-state response to the maximum value of the static tooth force during the same mesh cycle

$$(DF)_{tf} = \frac{(DTF)_{max}}{(STF)_{max}} \tag{10b}$$

Finally, the dynamic stress factor $(DF)_{\sigma}$ is defined as the ratio of the maximum value of the dynamic bending stress σ_d on the gear tooth in one complete mesh cycle of the steady-state response to the maximum value of the static bending stress σ_s during one mesh cycle

$$(DF)_{\sigma} = \frac{(\sigma_d)_{max}}{(\sigma_s)_{max}} \tag{10c}$$

Figures 10–12 compare these three types of DF predicted by both dynamic models to the predicted DTE values for the gear pairs used in Figs. 6–8, respectively. In these figures, the top figure displays $(DF)_{mf}$, $(DF)_{tf}$, and $(DF)_{\sigma}$ together with DTE as predicted by the deformable-body model while the bottom figure shows discrete model predictions of $(DF)_{mf}$, $(DF)_{tf}$, and DTE. $(DF)_{\sigma}$ is not included in the bottom figures since the discrete model is not capable of predicting stresses. In Figs. 10–12, the

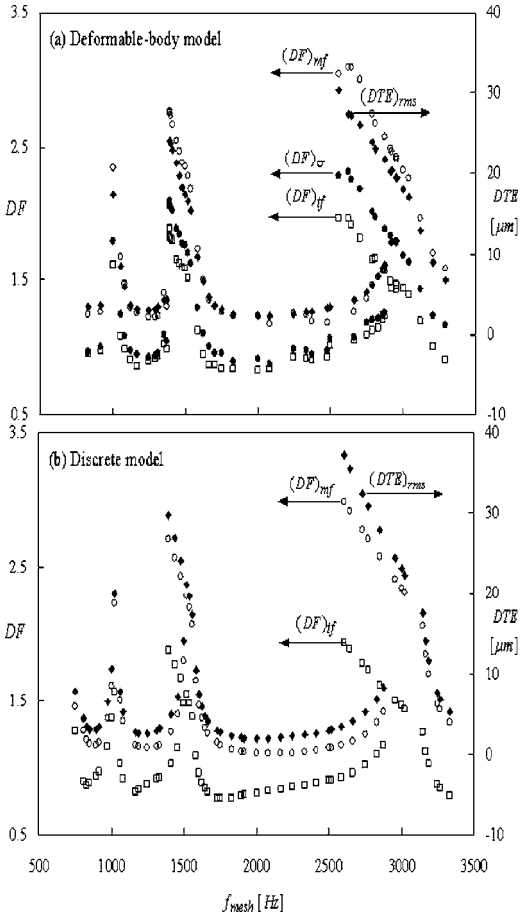

Fig. 10 Comparison of $(DF)_{mf}$, $(DF)_{tf}$, $(DF)_{\sigma}$, and $(DTE)_{rms}$ for an unmodified gear pair with δ=0 and ICR=1.8 at 340 Nm: (*a*) Deformable-body model and (*b*) discrete model

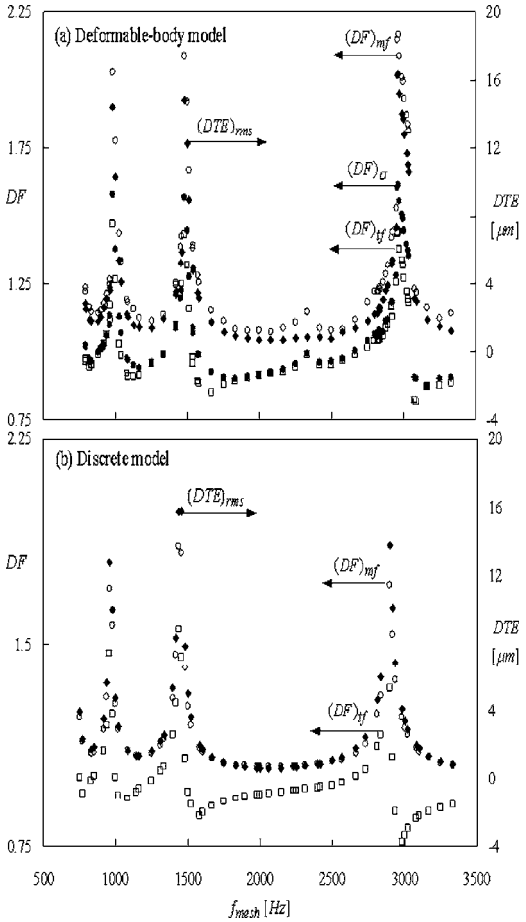

Fig. 11 Comparison of $(DF)_{mf}$, $(DF)_{tf}$, $(DF)_{\sigma}$, and $(DTE)_{rms}$ for a modified gear pair with δ=10 μm, α=20.9 deg, and ICR=1.8 at 340 Nm: (*a*) Deformable-body model and (*b*) discrete model

vertical axis for $(DF)_{mf}$, $(DF)_{tf}$, and $(DF)_{\sigma}$ is shown on the left-hand side and the vertical axis for DTE is to the right.

Focusing on the deformable-body model predictions first (Figs. 10(*a*), 11(*a*), and 12(*a*)), it is seen that (i) values of $(DF)_{tf}$ and $(DF)_{\sigma}$ are very close to each other regardless of the mesh frequency, and (ii) $(DF)_{mf}$ and rms values of DTE are proportional to each other. The first observation is somewhat expected since the tooth force and the resultant bending stress can be considered to be linearly proportional to each other, at least when only the tooth-bending effects are considered. It can also be stated that $(DF)_{mf}$ is always significantly larger than both $(DF)_{tf}$ and $(DF)_{\sigma}$. For instance, at 2750 Hz in Fig. 10, lower branch motion has $(DF)_{tf} \approx (DF)_{\sigma}=1.1$ and $(DF)_{mf}=1.4$. At the same frequency, the upper branch motion yields $(DF)_{tf}=1.8$, $(DF)_{\sigma}=2.0$ and $(DF)_{mf}=2.75$. At this frequency, a design based on $(DF)_{mf}$ would be about 25–35 % more conservative than a design based on $(DF)_{tf}$ or $(DF)_{\sigma}$. Considering that $(DF)_{tf}$ or $(DF)_{\sigma}$ are directly related the contact and bending failures of a gear tooth, prediction of previous discrete-parameter models that focused solely on $(DF)_{mf}$ might not be able to represent the actual dynamic loading conditions and, hence, dynamic fatigue loading, experienced at the tooth flank of a gear pair.

A comparison between the predictions of both models in Figs. 10–12 reveals that the discrete model is in good agreement with the deformable-body model in predicting DF. This has practical consequences since the discrete model is several orders of magnitude faster than the deformable-body model. Also considering that values $(DF)_{tf}$ and $(DF)_{\sigma}$ are rather close to each other, the discrete model can provide a dynamic factor that can be readily used for design purposes.

4.1 Relationships Between DTE and Different Forms of DF. In the previous section, DF values were shown to follow the same overall trends as DTE predictions as the mesh frequency is varied. This brings the possibility of establishing certain relationships between different forms of DF and DTE. If this can be accomplished, measurement of DTE, which is in many cases a more feasible task than measurement of DF especially for finer pitch gears, could be used as an indirect measure of DF for design purposes. This would also provide the well-established DTE database to be used for durability purposes. In this section, an attempt has been made to relate (i) DTE to $(DF)_{mf}$ and (ii) DTE to $(DF)_{\sigma}$. Since $(DF)_{tf}$ and $(DF)_{\sigma}$ have similar values, the second item would also relate DTE to $(DF)_{tf}$.

For the relationship between DTE and $(DF)_{mf}$, half of the peak-to-peak values of DTE and DMF, denoted by $(DTE)^{o\text{-}p}$ and $(DMF)^{o\text{-}p}$ were normalized with respect to λ and SMF, respectively. Here, δ corresponds to the difference between the average values of LSTE and unloaded STE given by $\lambda=(LSTE)_{ave}-e_{ave}$. These two normalized parameters at all mesh frequencies are plotted against each other in Fig. 13 for all the three gear pairs considered earlier as predicted by the discrete model. In these figures, the slope for the no contact loss solutions is nearly equal to unity and, hence,

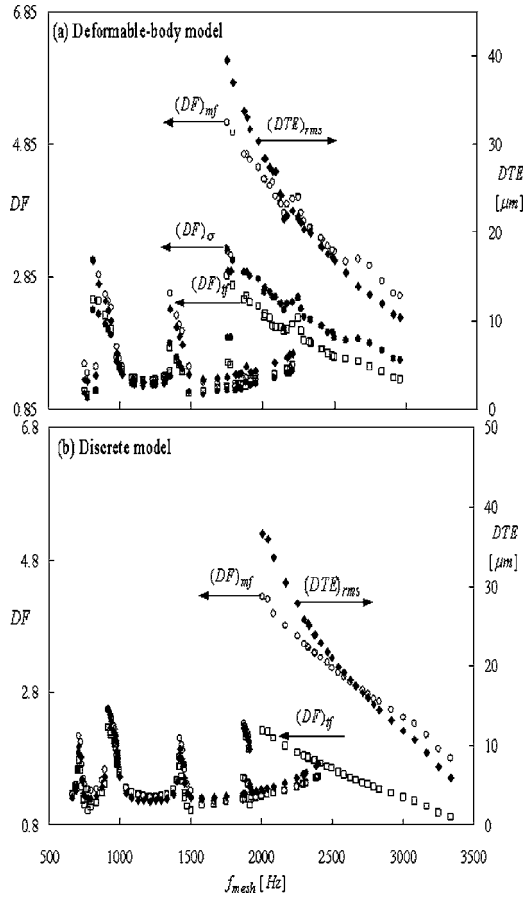

Fig. 12 Comparison of $(DF)_{mf}$, $(DF)_{tf}$, $(DF)_{\sigma}$, and $(DTE)_{rms}$ for an unmodified gear pair with δ=0 and ICR=1.4 at 170 Nm: (*a*) Deformable-body model and (*b*) discrete model

$$\frac{(\mathrm{DMF})^{o\text{-}p}}{\mathrm{SMF}} \approx \frac{(\mathrm{DTE})^{o\text{-}p}}{\lambda} \tag{11a}$$

Rearranging this equation as

$$\frac{(\mathrm{DMF})^{o\text{-}p} + \mathrm{SMF}}{\mathrm{SMF}} \approx \frac{(\mathrm{DTE})^{o\text{-}p}}{\lambda} + 1 \tag{11b}$$

letting $(\mathrm{DMF})^{o\text{-}p}+\mathrm{SMF}=(\mathrm{DMF})_{\max}$, and using the earlier definition of $(\mathrm{DF})_{mf}$ given by Eq. (10*a*), one writes the first relationship of interest as

$$(\mathrm{DF})_{mf} \approx \frac{(\mathrm{DTE})^{o\text{-}p}}{\lambda} + 1 \tag{12}$$

This relationship between $(\mathrm{DF})_{mf}$ and DTE is quite accurate in the linear frequency ranges when no contact loss occurs, but would give a conservative estimate $(\mathrm{DF})_{mf}$ in the nonlinear regime. This is evident in Figs. 13(*a*) and 13(*c*) for the regions of tooth separation where the slope is nearly one-half. As a matter of fact, Eq. (11*a*) can be rewritten as

$$(\mathrm{DMF})^{o\text{-}p} = \left[\frac{\mathrm{SMF}}{\lambda}\right](\mathrm{DTE})^{o\text{-}p} \tag{13}$$

where the slope can be physically interpreted as the average value of stiffness. In the nonlinear region, because the teeth separate during a portion of the mesh cycle, the average value of stiffness is reduced. Hence, the decrease in slope observed in Figs. 13(*a*) and 13(*c*) should be expected.

The second relationship between $(\mathrm{DF})_{\sigma}$ and DTE is illustrated with the help of Figs. 14(*a*)–14(*c*) obtained by using the predictions of the deformable body model for the same three gear pairs. These figures plot $(\mathrm{DF})_{\sigma}$ against $(\mathrm{DTE})_{\max}$ that is normalized with respect to $(\mathrm{LSTE})_{\max}$. Figures 14 demonstrate a direct linear relationship between these two parameters such that

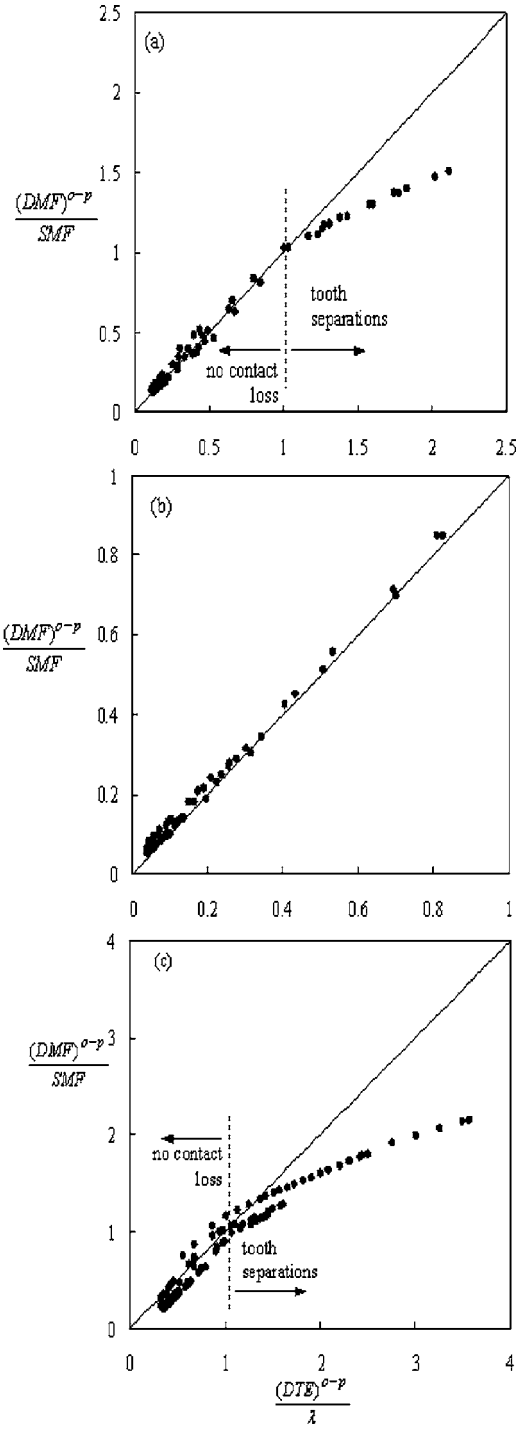

Fig. 13 Normalized values of $(\mathrm{DMF})^{o\text{-}p}$ versus $(\mathrm{DTE})^{o\text{-}p}$ for (*a*) δ=0, ICR=1.8, (*b*) δ=10 μm, α=20.9 deg, ICR=1.8, and (*c*) δ=0, ICR=1.4

$$(\mathrm{DF})_{\sigma} = \frac{(\mathrm{DTE})_{\max}}{(\mathrm{LSTE})_{\max}} \tag{14}$$

This relationship provides a very good approximation for $(\mathrm{DF})_{\sigma}$ in both linear and nonlinear regimes and can be used for design purposes in estimating $(\mathrm{DF})_{\sigma}$ from DTE.

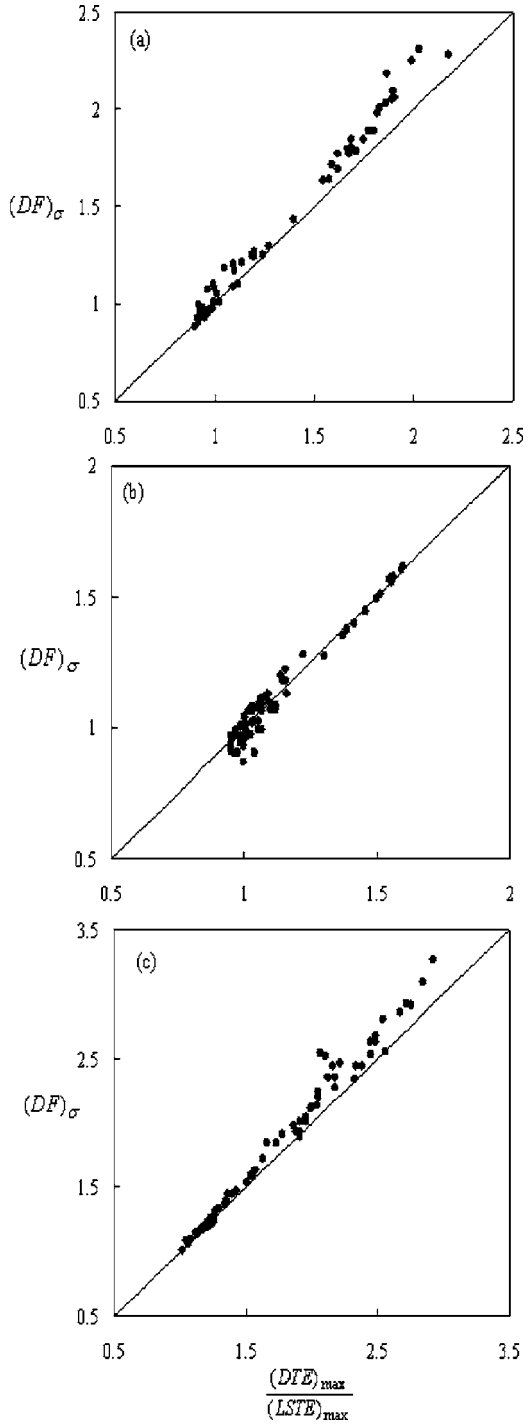

Fig. 14 $(DF)_\sigma$ versus $(DTE)_{max}$ for (*a*) δ=0, ICR=1.8, (*b*) δ =10 μm, α=20.9 deg, ICR=1.8, and (*c*) δ=0, ICR=1.4

5 Conclusion

In this study, two different dynamic models of varying complexity were developed and validated by comparing the predicted DTE values to the available experimental data. The deformable-body model is capable of predicting DTE, tooth forces, as well as the tooth-bending stresses. The discrete model uses the results from the quasi-static analysis of the deformable-body model to predict the DTE, and gear mesh and tooth forces. Three different dynamic factors were defined and their values were compared with that of DTE in both linear and nonlinear motion regimes. Dynamic factors based on tooth forces and bending stresses were shown to be approximately equal, whereas dynamic factors based on total gear mesh forces are consistently higher that the other two types of dynamic factors. At the end, simple design formulas were proposed to relate DTE to dynamic factors based on gear mesh forces and stresses.

Nomenclature

b = backlash
$\mathbf{C}$ = damping matrix
c = viscous damping coefficient
DF = dynamic factor
DMF = dynamic mesh force
DTE = dynamic transmission error
DTF = dynamic tooth force
e = displacement excitation (unloaded static transmission error)
F = force
g = nonlinear function
I = polar mass moment of inertia
ICR = involute contact ratio
$\mathbf{K}$ = stiffness matrix
k = stiffness
LSTE = loaded static transmission error
$\mathbf{M}$ = mass matrix
m = mass
r = base radius
SMF = static mesh force
STE = static transmission error
STF = static tooth force
T = torque
α = roll angle
δ = tip relief magnitude
η, μ = Rayleigh's stiffness and mass damping coefficients
θ = alternating component of the rotational displacement
σ = bending stress
ζ = damping ratio
τ = dimensionless time
ω = frequency

Subscripts

1, 2 = pinion and gear
a = alternating component
ave = average
d = dynamic
f = deflection component
m = mean component
max, min = maximum and minimum values
mf, tf = mesh force, tooth force
r = rigid body component
rms = root mean square value
s = static
σ = bending stress

Superscripts

o-p = half of peak to peak value

References

[1] American National Standard, "Fundamental Rating Factors and Calculation Methods for Involute Spur and Helical Gear Teeth," *AGMA Standard, ANSI/AGMA 2001-C95*.
[2] Ozguven, H. N., and Houser, D. R., 1988, "Mathematical Models Used in Gear Dynamics—A Review," J. Sound Vib., **121**, pp. 383–411.
[3] Blankenship, G. W., and Singh, R., 1992, "A Comparative Study of Selected Gear Mesh Interface Dynamic Models," ASME International Power Transmission and Gearing Conference, DE 43-1.
[4] Wang, J., Li, R., and Peng, X., 2003, "Survey of Nonlinear Vibration of Gear Transmission Systems," Appl. Mech. Rev., **56**(3), pp. 309–329.
[5] Kahraman, A., Ozguven, H. N., Houser, D. R., and Zakrajsek, J. J., 1992, "Dynamic Analyses of Geared Rotors by Finite Elements," ASME J. Mech.

Des., **114**, pp. 507–514.
[6] Ozguven, H. N., and Houser, D. R., 1988, "Dynamic Analysis of High Speed Gears by Using Loaded Static Transmission Error," J. Sound Vib., **125**, pp. 71–83.
[7] Ozguven, H. N., 1991, "A Non-linear Mathematical Model for Dynamic Analysis of Spur Gears Including Shaft and Bearing Dynamics," J. Sound Vib., **145**, pp. 239–260.
[8] Kahraman, A., and Singh, R., 1990, "Non-linear Dynamics of a Spur Gear Pair," J. Sound Vib., **142**, pp. 49–75.
[9] Amabili, M., and Rivola, A., 1997, "Dynamic Analysis of Spur Gear Pairs: Steady-State Response and Stability of the SDOF Model With Time-varying Mesh Damping," Mech. Syst. Signal Process., **11**, pp. 375–390.
[10] Huang, K. J., and Liu, T. S., 2000, "Dynamic Analysis of a Spur Gear by the Dynamic Stiffness Method," J. Sound Vib., **234**(2), pp. 311–329.
[11] Theodossiades, S., and Natsiavas, S., 2000, "Non-linear Dynamics of Gear-Pair Systems With Periodic Stiffness and Backlash," J. Sound Vib., **229**(2), pp. 287–310.
[12] Maliha, R., Dogruer, U., and Ozguven, H. N., 2004, "Nonlinear Dynamic Modeling of Gear-Shaft-Disk-Bearing Systems Using Finite Elements and Describing Functions," ASME J. Mech. Des., **126**, pp. 534–541.
[13] Blankenship, G. W., and Singh, R., 1995, "A New Gear Mesh Interface Dynamic Model to Predict Multi-Dimensional Force Coupling and Excitation," Mech. Mach. Theory, **30**(1), pp. 43–57.
[14] Munro, R. G., 1962, "Dynamic Behaviour of Spur Gears," Ph.D. dissertation, Cambridge University.
[15] Umezawa, K., Sata, T., and Ishikawa, J., 1984, "Simulation of Rotational Vibration of Spur Gears," Bull. JSME, **27**, pp. 102–109.
[16] Blankenship, G. W., and Kahraman, A., 1995, "Steady State Forced Response of a Mechanical Oscillator With Combined Parametric Excitation and Clearance Type Nonlinearity," J. Sound Vib., **185**, pp. 743–765.
[17] Kahraman, A., and Blankenship, G. W., 1996, "Interactions Between Commensurate Parametric and Forcing Excitations in a System With Clearance," J. Sound Vib., **194**, pp. 317–336.
[18] Kahraman, A., and Blankenship, G. W., 1997, "Experiments on Nonlinear Dynamic Behavior of an Oscillator With Clearance and Time-Varying Parameters," ASME J. Appl. Mech., **64**, pp. 217–226.
[19] Kahraman, A., and Blankenship, G. W., 1999, "Effect of Involute Tip Relief on Dynamic Response of Spur Gear Pairs," ASME J. Mech. Des., **121**, pp. 313–315.
[20] Kahraman, A., and Blankenship, G. W., 1999, "Effect of Involute Contact Ratio on Spur Gear Dynamics," ASME J. Mech. Des., **121**, pp. 112–118.
[21] Kasuba, R., and Evans, J. W., 1981, "An Extended Model for Determining Dynamic Loads in Spur Gearing," ASME J. Mech. Des., **100**, pp. 69–76.
[22] Wang, C. C., 1985, "On Analytical Evaluation of Gear Dynamic Factors Based on Rigid Body Dynamics," Journal of Mechanisms, ASME J. Mech., Transm., Autom. Des., **107**, pp. 301–311.
[23] Lin, H. H., Oswald, F. B., and Townsend, D. P., 1994, "Dynamic loading of Spur Gears with Linear or Parabolic Tooth Profile Modifications," Mech. Mach. Theory, **29**(8), pp. 1115–1129.
[24] Liou, C. H., Lin, H. H., Oswald, F. B., and Townsend, D. P., 1996, "Effect of Contact Ratio on Spur Gear Dynamic Load With No Tooth Profile Modifications," ASME J. Mech. Des., **118**, pp. 439–443.
[25] Yoon, K. Y., and Rao, S. S., 1996, "Dynamic Load Analysis of Spur Gears Using a New Tooth Profile," ASME J. Mech. Des., **118**, pp. 1–6.
[26] Vedmar, L., and Henriksson, B., 1998, "A General Approach for Determining Dynamic Forces in Spur Gears," ASME J. Mech. Des., **120**, pp. 593–598.
[27] Vedmar, L., and Andersson, A., 2003, "A Method to Determine Dynamic Loads on Spur Gear Teeth and on Bearings," J. Sound Vib., **267**, pp. 1065–1084.
[28] Parker, R. G., Vijayakar, S. M., and Imajo, T., 2000, "Non-linear Dynamic Response of a Spur Gear Pair: Modeling and Experimental Comparison," J. Sound Vib., **237**, pp. 435–455.
[29] Kubo, A., Yamada, K., Aida, T., and Sato, S., 1972, "Research on Ultra High Speed Gear Devices," Trans. Jpn. Soc. Mech. Eng., **38**, pp. 2692–2715.
[30] *EXTPAIR-2D User's Manual*, Advanced Numerical Solutions, Inc., Columbus, OH, 2004.
[31] Vijayakar, S., Busby, H. R., and Houser, D. R., 1987, "Finite Element Analysis of Quasi-prismatic Bodies Using Chebyshev Polynomials," Int. J. Numer. Methods Eng., **24**, pp. 1461–1477.
[32] Yuksel, C., and Kahraman, A., 2004, "Dynamic Tooth Loads of Planetary Gear Sets Having Tooth Profile Wear," Mech. Mach. Theory, **39**, pp. 695–715.
[33] Tamminana, V. K., "An Investigation of the Relationship Between the Dynamic Transmission Error and Dynamic Factors of a Spur Gear Pair," M.S. thesis, The Ohio State University, Columbus, 2005.